

# Deep Learning for Direction of Arrival Estimation via Emulation of Large Antenna Arrays

Aya Mostafa Ahmed<sup>\*</sup>, *Student Member, IEEE*, Udaya Sampath K.P. Miriya Thantrige<sup>\*</sup>, *Student Member, IEEE*, Aly El Gamal, *Senior Member, IEEE*, and Aydin Sezgin, *Senior Member, IEEE*

**Abstract**—We present a MUSIC-based Direction of Arrival (DOA) estimation strategy using small antenna arrays, via employing deep learning for reconstructing the signals of a virtual large antenna array. Not only does the proposed strategy deliver significantly better performance than simply plugging the incoming signals into MUSIC, but surprisingly, the performance is also better than directly using an actual large antenna array with MUSIC for high angle ranges and low test SNR values. We further analyze the best choice for the training SNR as a function of the test SNR, and observe dramatic changes in the behavior of this function for different angle ranges.

**Index Terms**—MUSIC algorithm, sparse antenna array, angle of arrival, deep neural network, training SNR.

## I. INTRODUCTION

Direction of arrival (DOA) estimation refers to estimating the direction of several target electromagnetic waves through receive antennas that form a *sensor array*. DOA has a wide range of applications, e.g., radar, sonar, and wireless communications [1]. Accurate DOA estimation can be achieved using large antenna arrays at the cost of increased hardware and computational complexity. However, multiple input multiple output (MIMO) radars with co-located antennas can offer virtual enlargement of the aperture at the receiver, using relatively few physical antennas. This in turn significantly increases the maximum number of targets that could be detected, and enhances the angular resolution at a compact size. This is due to the fact that MIMO radars can transmit multiple probing signals, which can be correlated or uncorrelated [2], [3]. As an alternative approach, sparse array radars (also known as thin array radars) have been extensively studied in the literature and found to offer similar advantages as MIMO radars [4]. The idea is to decompose a filled array into two sub-arrays, breaking the uniform spacing rule, hence achieving a larger aperture. By this means, it can offer similar target detection and angular resolution capabilities as the MIMO radar [5] with lower hardware cost. For this purpose, several array configurations were proposed in the literature [6], [7], [8]. However, sparse arrays suffer from the effect of grating lobes

due to the non-uniform spacing between the antennas, which leads to large estimation errors [9]. Furthermore, existing vector space DOA methods such as the Multiple-Signal Classification (MUSIC) algorithm can not be directly applied, due to the rank deficiency of the correlation matrix. Hence, a spatial smoothing variant of MUSIC is proposed in [10] for rank enhancement at the cost of increased computational cost. This is due to the fact that spatial smoothing must be performed for every DOA estimation.

A comparison between MIMO and sparse array radars has been conducted in [4], where MIMO radars were found to be preferable when compactness is essential, since sparse arrays are characterized by their large aperture size. However, sparse arrays might be preferable when the hardware costs is the driving requirement, yet sparse arrays are not robust to sensor failures unlike uniform linear arrays (ULA) [11], which could present an added challenge. In this work, we investigate a novel approach which enhances the angular resolution and target detection capacity while satisfying both low cost and compactness properties. We exploit the potential of deep neural networks to learn the mapping between two antenna arrays of different sizes. More specifically, we try to emulate the received signal of a large ULA using only a significantly smaller sub-array, without the need to increase the array aperture size. Such mapping is done through training a deep neural network. This is followed by using the trained model for each received pulse to estimate the DOA via employing state of the art MUSIC without any further processing. Such approach delivers the advantages of sparse arrays (i.e. hardware cost reduction) without increasing the aperture size, and without compromising accuracy. Furthermore, no additional computational cost is required as MUSIC can be directly applied without spatial smoothing.

## II. SYSTEM MODEL

Consider a co-located MIMO radar system with  $M$  transmit (TX) antennas and  $N$  receive (RX) antennas. Here, each transmit antenna with index  $m$  transmits a narrow-band signal  $s_m(t)$  with nondispersive propagation, that is perfectly orthogonal to the rest and consists of a train of  $P$  non-overlapping pulses; each with duration  $T$ . For simplicity, we consider TX and RX antennas in a ULA configuration with antenna spacing of  $d = \lambda/2$ , where  $\lambda$  is the wavelength. We further assume that there are  $K$  targets in the scene. The radar cross section (RCS) - based on pulse  $p$  - and the direction of arrival (DOA) of the  $k$ -th target are given by  $\alpha_{k,p} \in \mathbb{C}$  and  $\theta_k$ , respectively. In

This work is funded by the Deutsche Forschungsgemeinschaft (DFG, German Research Foundation) project-id287022738 TRR 196 (S02 and S03)

A. M. Ahmed, U. S. K. P. M. Thantrige, and A. Sezgin are with the Institute of Digital Communication Systems, Ruhr University Bochum, 44801 Bochum, Germany (e-mail: aya.mostafaibrahimahmad@rub.de; udaya.miriyathantrige@rub.de; aydin.sezgin@rub.de).

A. El Gamal is with the Department of Electrical and Computer Engineering, Purdue University, West Lafayette, IN, USA. e-mail: elgamala@purdue.edu

<sup>\*</sup> These authors contributed equally to the work

this paper, the target RCS is modeled based on the Swerling model II, where it is fixed during the pulse interval  $T$  and changes independently from one pulse interval to another [12]. We define the transmit and receive steering vectors of the  $k$ -th target as  $\mathbf{a}_t(\theta_k) = [1, e^{j\rho d \sin \theta_k}, \dots, e^{j\rho d(M-1) \sin \theta_k}]^T$  and  $\mathbf{a}_r(\theta_k) = [1, e^{j\rho d \sin \theta_k}, \dots, e^{j\rho d(N-1) \sin \theta_k}]^T$ , respectively. Here,  $(\cdot)^T$  is the transpose, and  $\rho = \frac{2\pi}{\lambda}$ . Here, we consider all targets as point targets. In that case, the received echo (reflected signal) from the target does not expand beyond the radar resolution cell [13]. Based on the point target assumption, the received signal  $\mathbf{r}(t) \in \mathbb{C}^N$ , after transmitting  $P$  pulses is [2]

$$\mathbf{r}(t) = \sum_{k=1}^K \sum_{p=1}^P \alpha_{k,p} \mathbf{a}_r(\theta_k) \mathbf{a}_t^T(\theta_k) \mathbf{s}(t - pT) + \mathbf{n}(t), \quad (1)$$

where  $\mathbf{n}(t) \in \mathbb{C}^N$  is independent and identically distributed (i.i.d) Gaussian noise with variance  $\sigma^2$  and  $\mathbf{s}(t) = [s_1(t), \dots, s_m(t)]^T$ . Next, at each receive antenna, the received signal  $\mathbf{r}(t)$  is cross-correlated with  $M$  matched filters corresponding to each transmit signal as given below

$$\mathbf{Z}_p(t) = \int_0^T \mathbf{r}(t) \mathbf{s}^H(t - pT) dt. \quad (2)$$

Here,  $(\cdot)^H$  is the conjugate transpose. Due to the perfect orthogonality of the transmit waveforms,  $\mathbf{Z}_p(t)$  in (2) is given as

$$\mathbf{Z}_p(t) = \sum_{k=1}^K \sum_{p=1}^P \alpha_{k,p} \mathbf{a}_r(\theta_k) \mathbf{a}_t^T(\theta_k) \mathbf{I} + \int_0^T \mathbf{n}(t) \mathbf{s}^H(t - pT) dt. \quad (3)$$

Here,  $\mathbf{I}$  is an identity matrix. Next, we rearrange (3) in matrix format as given below

$$\mathbf{Y} = \mathbf{A}(\theta) \mathbf{X} + \mathbf{N}. \quad (4)$$

To this end,  $\mathbf{Y} \in \mathbb{C}^{MN \times P}$  is the receive signal and it is given as  $\mathbf{Y} = [\text{vec}(\mathbf{Z}_1), \dots, \text{vec}(\mathbf{Z}_P)]$ . Here,  $\text{vec}(\mathbf{Z}_p)$  denotes the conversion of the matrix  $\mathbf{Z}_p$  of (3) into a column vector. The steering vector matrix  $\mathbf{A}(\theta)$  is given by  $[\mathbf{v}(\theta_1), \dots, \mathbf{v}(\theta_K)]$ , where  $\mathbf{v}(\theta_k) = \mathbf{a}_r(\theta_k) \otimes \mathbf{a}_t(\theta_k)$ . Further, the RCS matrix  $\mathbf{X} \in \mathbb{C}^{K \times P}$  corresponding to all  $K$  targets is given as  $\mathbf{X} = [\mathbf{x}_1, \dots, \mathbf{x}_P]$ , with  $\mathbf{x}_p = [\alpha_{1,p}, \dots, \alpha_{K,p}]^T$ . In the next section, we introduce the proposed deep neural network (DNN) based signal prediction approach. Here, our objective is to find a mapping between the received signals  $\mathbf{Y}$  of (4) corresponding to two different antenna setups.

### III. DEEP LEARNING ARCHITECTURE

The enlargement of the antenna array aperture enhances the angular resolution capabilities of the radar which in turn leads to a better DOA estimation. Hence, we aim in this section to improve the performance of an antenna array through emulating a larger aperture ULA. For this matter, we tackle the problem of mapping the received signal of two antenna setups of different sizes. Hence, a feed forward deep neural network (DNN) is proposed, whose goal is to learn the mapping between the received signals of low and

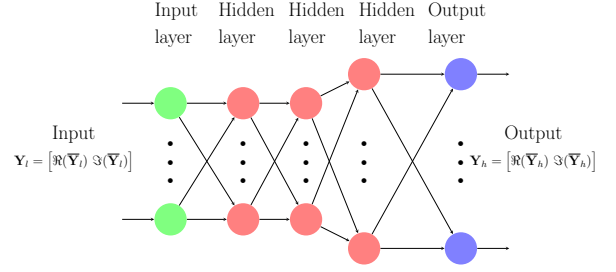


Fig. 1: Training the Deep Neural Network.

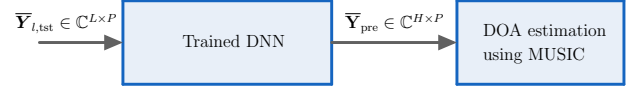


Fig. 2: Antenna array reconstruction using the DNN.

high antenna setups. Let  $\bar{\mathbf{Y}}_l \in \mathbb{C}^{L \times P}$  and  $\bar{\mathbf{Y}}_h \in \mathbb{C}^{H \times P}$  be the received signals of the low and high antenna setups as defined in (4), respectively. Here,  $L = M_l N_l < H = M_h N_h$ . This is done through training a DNN consisting of four fully connected layers, where the input layer is of dimension  $L$ , followed by three hidden layers of dimensions  $L, L$ , and  $H$ , respectively, and the output layer is of dimension  $H$ . The DNN architecture is shown in Fig. 1. We chose the smallest network that led to good performance in our experiments to reduce the associated computational complexity. Since the DNN is not designed for special processing of complex data, the input and output are defined as  $\mathbf{Y}_l = [\Re(\bar{\mathbf{Y}}_l); \Im(\bar{\mathbf{Y}}_l)]$ , and  $\mathbf{Y}_h = [\Re(\bar{\mathbf{Y}}_h); \Im(\bar{\mathbf{Y}}_h)]$ , where  $\Re(\cdot)$ , and  $\Im(\cdot)$  denote the real and imaginary components, respectively. Both received and reconstructed signals are normalized to lie between 0 and 1 through min-max normalization. ReLU is used as an the activation function for all the hidden layers. For the output layer, we tried both linear activation and ReLU, and then we chose the best performance for each experiment. The available dataset is divided into training, validation and testing, with split ratios of 60%, 20% and 20%, respectively. Training takes place over a maximum of 150 epochs with a batch size of 120. For the training process, we used an Adam optimizer with the mean squared error loss function. In the testing phase, the DNN is tested using  $\mathbf{Y}_{l,\text{tst}} \in \mathbb{R}^{2L \times P}$ , where it predicts  $\mathbf{Y}_{\text{pre}} \in \mathbb{R}^{2H \times P}$ , as shown in Fig. 2. DOA estimation is calculated from the predicted received signal  $\bar{\mathbf{Y}}_{\text{pre}} \in \mathbb{C}^{H \times P}$  through the MUSIC algorithm. The covariance matrix is calculated using only 100 received signals (i.e., 100 snapshots) as

$$\begin{aligned} \mathbf{R}_{\text{pre}} &= \mathbb{E}[\bar{\mathbf{Y}}_{\text{pre}} \bar{\mathbf{Y}}_{\text{pre}}^H] = \mathbf{A}(\theta) \mathbb{E}[\mathbf{X} \mathbf{X}^H] \mathbf{A}^H(\theta) + \sigma^2 \mathbf{I}, \\ &= \mathbf{U}_x \mathbf{\Lambda}_x \mathbf{U}_x^H + \mathbf{U}_n \mathbf{\Lambda}_n \mathbf{U}_n^H, \end{aligned} \quad (5)$$

where  $\mathbb{E}[\cdot]$  denotes the expected value,  $\mathbf{U}_x$  and  $\mathbf{U}_n$  are matrices containing the eigenvectors, which represent the signal and noise subspaces, respectively.  $\mathbf{\Lambda}_x = \text{diag}(\lambda_1, \dots, \lambda_K)$  and  $\mathbf{\Lambda}_n = \text{diag}(\lambda_{K+1}, \dots, \lambda_{MN})$  contain the corresponding eigenvalues of the target and the noise, respectively. Hence,

$N_l = M_l$	10	$N_h = M_h$	16
Angle grid 1	0 : 25	Angle grid 2	20 : 45
Angle grid 3	40 : 65	Number of targets ( $K$ )	4

TABLE I: Simulation Parameters

the expression of the MUSIC spectrum which provides the received signal energy distribution for all receive directions is given by  $P_{MU}(\theta) = (\mathbf{v}^H(\theta)\mathbf{U}_n\mathbf{U}_n^H\mathbf{v}(\theta))^{-1}$ . For a comprehensive evaluation of our model performance, we define two metrics. First, we define the covariance matrix error as

$$R_e = \|\mathbf{R}_{h,\text{tst}} - \mathbf{R}_{\text{pre}}\|_F, \quad (6)$$

where  $\|\cdot\|_F$  is the Frobenius norm,  $\mathbf{R}_{h,\text{tst}} = \mathbb{E}[\bar{\mathbf{Y}}_{h,\text{tst}}\bar{\mathbf{Y}}_{h,\text{tst}}^H]$ , and  $\bar{\mathbf{Y}}_{h,\text{tst}}$  is the received signal of the high antenna setup during inference. The analysis of the covariance matrix of the received signal has a significant importance here as it is directly used to calculate the MUSIC spectrum. Second, to evaluate the DOA estimation performance, the average normalized root mean squared error (RMSE) is used as the performance metric. For a single DOA estimation, the normalized root mean squared error is given by  $RMSE_s = \sqrt{\frac{1}{K} \sum_{k=1}^K (\hat{\theta}_k - \theta_k)^2 / \sum_{k=1}^K (\theta_k)^2}$ . Here, the estimated and actual angles of the  $k$ -th target are given as  $\hat{\theta}_k$  and  $\theta_k$ , respectively. Finally, for a number of DOA estimations equals  $Q$ , the average normalized root mean squared error (RMSE) is given by  $RMSE = (\sum_{s=1}^Q RMSE_s) / Q$ .

#### IV. SIMULATION RESULTS

To train the DNN, we use a server with 32 GB memory and a single GPU (NVIDIA Quadro RTX 5000). In all simulations, we consider 10000 data samples for testing in each angle range (by setting  $P$  in (4)). Other parameters that are used in the simulations are listed in Table I. We separately consider multiple angle ranges, which span the scope of the incident signal. Due to space limitations, we consider here only three angle ranges, however similar results were obtained for others. Each range is chosen to span 25 degrees to place the targets. Also, here we set the minimum spatial distance of five degrees between two targets to ensure the best spatial resolution of the actual large antenna setup of  $16 \times 16$  antennas.

##### A. Initial Performance Analysis

Different training sets are considered in the training phase. Specifically, we consider 16 datasets<sup>1</sup> with different SNR combinations. Here, two datasets (M1 and M2) contain data with a mix of SNR values while the other 14 datasets involve only a single SNR each. M1 and M2 contain equal percentage of data samples from each training SNR ( $\text{SNR}_{\text{train}}$ ) ranging from -16 dB to 10 dB with a step size of 2 dB. The only difference in constructing these two datasets is the size, as they consist of 560000 and 40000 samples, respectively. Furthermore, each of the other 14 datasets consists of 40000 samples. For the testing phase, we estimate the DOA for 10000 samples in the testing SNR ( $\text{SNR}_{\text{test}}$ ) range of -16...10

<sup>1</sup>Source code is available for download at <https://gitlab.com/miriyugl/doa-with-dnn-via-emulation-of-antenna-arrays>

dB with the same training step size. The average normalized RMSEs for different training datasets are shown in Fig. 3. In this figure, DOA estimation using the predicted signal of the DNN is compared with the DOA estimation obtained by directly using the signals obtained from the actual low and high antenna setups. Three cases for the DNN prediction task are explored in this figure:

- Case 1: Training the DNN with the M2 dataset (i.e., mix of SNR values while retaining single SNR dataset size).
- Case 2: Training the DNN with the same SNR as that used in testing (e.g., using the DNN model trained with  $\text{SNR}_{\text{train}} = -16$  dB at  $\text{SNR}_{\text{test}} = -16$  dB)
- Case 3: Selecting the lowest RMSE of DOA estimation achieved across all 16 data sets for each testing SNR (e.g. using the DNN model trained with  $\text{SNR}_{\text{train}} = -8$  dB leads to the lowest RMSE at  $\text{SNR}_{\text{test}} = -16$  dB for the angle range of 20 – 45 degrees).

Now, Fig. 3 shows that the predicted signal typically leads to better performance than directly using the signal of the low antenna setup ( $10 \times 10$ ), specially in the low SNR regime and for high angle ranges. One exception is observed for the DNN prediction compared to the low antenna setup in high SNR regimes for the low angle range in Fig. 3(a). Here, the low antenna setup performs slightly better compared to the DNN prediction. Fig. 3 also demonstrates that training and testing with the same SNR closely follows the best achievable performance, and hence highlighting the impact of knowing the test SNR value and choosing the simple strategy of training at only that value. In addition, Fig. 3 demonstrates the difference in behavior among different angle ranges. More specifically, the performance of the DOA estimation obtained from using the signals corresponding to the actual antenna setups becomes worse for higher angle ranges. We believe that this is due to the loss of spatial resolution of the ULA as the target directions shift to the endfire direction of the antenna array (i.e.  $|\theta_k| \geq 60$ ). This is due to the fact that in this range, the beam sharpness reduces remarkably as the effective array aperture decreases towards those directions [14]. Interestingly, as we observe in Fig. 3(c) for the higher angle range of 40–65 degrees, DOA estimation using our DNN-emulated signal outperforms the one generated using the actual high antenna setup in the low SNR regime. A possible explanation of this behavior is that, while pursuing improvement in generalization performance, the DNN performs denoising to the received signal. We further examine this hypothesis by evaluating  $R_e$  as defined in (6). Then, we compare the predicted signal with the actual received signal at a certain SNR offset. Hence, we define  $R_{\text{offset}}$  as

$$R_{\text{offset}} = \|\mathbf{R}_{h_o,\text{tst}} - \mathbf{R}_{\text{pre}}\|_F, \quad (7)$$

where  $\mathbf{R}_{h_o,\text{tst}} = \mathbb{E}[\bar{\mathbf{Y}}_{h_o,\text{tst}}\bar{\mathbf{Y}}_{h_o,\text{tst}}^H]$ , and  $\bar{\mathbf{Y}}_{h_o,\text{tst}}$  is the actual received signal at a certain SNR offset (e.g. if  $\bar{\mathbf{Y}}_{h,\text{tst}}$  and  $\bar{\mathbf{Y}}_{\text{pre}}$  are evaluated using  $\text{SNR}_{\text{test}} = -16$  dB, then  $\bar{\mathbf{Y}}_{h_o,\text{tst}}$  is evaluated using  $\text{SNR}_{\text{test}} = -8$  dB with an offset of 8 dB). In Fig. 4, we plot  $R_e$  and  $R_{\text{offset}}$  using the training datasets in cases 1 and 2 with offset values of 12 and 8 dB, respectively. Those offset values are chosen based on the observed performance

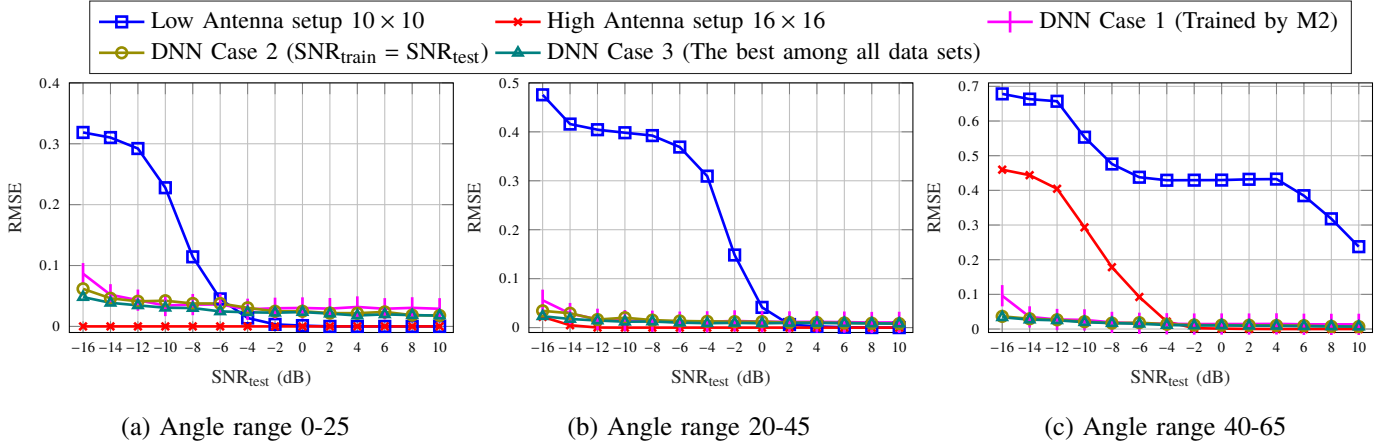


Fig. 3: DOA estimation comparison of the DNN based signal prediction for angle ranges 0 – 25, 20 – 45 and 40 – 65 degrees.

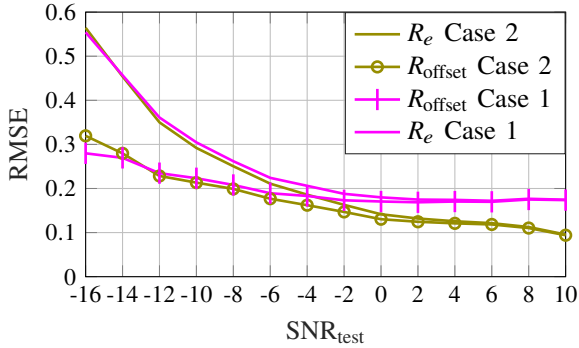


Fig. 4: RMSE of covariance matrix of predicted received signal compared to the actual high antenna setup at the same SNR and with SNR offset with ReLU output activation function.

corresponding to both cases. Fig. 4 shows that  $R_{\text{offset}}$  has much lower values compared to  $R_e$  in both cases. That signifies the statistical similarity between the predicted signal of the DNN and the less noisy version of the actual received signal of the high antenna setup. Further, as the SNR increases,  $R_{\text{offset}}$  and  $R_e$  converge to the same value. This underlines the validity of the hypothesis that the DNN denoises the received signal.

### B. What is the best training SNR range?

We first investigate the performance when training with a single SNR value across all testing SNR values. Fig. 5 shows the cumulative average normalized RMSEs of the DOA estimation over all testing SNRs for each training SNR. As an example, in Fig. 5(a), the bar corresponding to  $\text{SNR}_{\text{train}} = -10$  dB shows the summation of all RMSE values corresponding to the range  $\text{SNR}_{\text{test}} = [-16, \dots, 10]$  dB for the DNN trained with the -10 dB training set for the angle range of 0 – 25 degrees. Note that the shortest bar corresponds to the training SNR which provides the lowest cumulative RMSE over all testing SNR values. We observe that the training set M1 consistently provides the lowest cumulative RMSE. However, it may be difficult in practice to acquire - and train with -

a large dataset due to latency and computational constraints. Interestingly, training with the M2 set, that contains a mix of all considered training SNR values and has the same size as the considered single SNR training sets, leads to very good overall performance. Further, the best training SNR value, in terms of cumulative RMSE, **shifts from 0 dB for smaller angle ranges to negative SNR values for larger angle ranges**. Perhaps counterintuitively, training with high SNR values leads to mild performance in presence of uncertainty about the testing SNR. Inspired by the work in [15], further analysis is conducted to elaborate the relationship between the training and test SNR, and the results are shown in Fig. 6. Here, we investigate the suitable SNR range that can be used to train the DNN for each testing SNR. Let the testing and training SNR sets be given as  $\Omega_{\text{test}} = \{-16, -14, \dots, 8, 10 \text{ dB}\}$  and  $\Omega_{\text{train}} = \{M2, -16, -14, \dots, 8, 10 \text{ dB}\}$ , respectively. We then define the average normalized RMSE of the DOA estimation for the  $i^{\text{th}}$  training SNR corresponding to the  $j^{\text{th}}$  testing SNR as  $\text{RMSE}_{i,j}$ , where  $i \in \Omega_{\text{train}}$  and  $j \in \Omega_{\text{test}}$ . Next, we define the best training SNR - with lowest RMSE - for the  $j^{\text{th}}$  testing SNR as  $\text{RMSE}_{b,j} = \min_{i \in \Omega_{\text{train}}} \{\text{RMSE}_{i,j}\}$ . Furthermore, we define the set of SNR values for the  $j^{\text{th}}$  testing SNR  $\Omega_{j,tr}$  which contains the training SNRs whose DOA RMSE deviates by no more than 10% from the lowest RMSE as

$$\Omega_{j,tr} = \left\{ i \mid \left| \frac{\text{RMSE}_{i,j} - \text{RMSE}_{b,j}}{\text{RMSE}_{b,j}} \right| \leq 0.1, i \in \Omega_{\text{train}} \right\}. \quad (8)$$

Fig. 6 illustrates the values of  $\Omega_{j,tr}$  for the considered angle ranges. In Fig. 6,  $\blacktriangle$  and  $\blacksquare$  represent the best and the second best training SNRs ( $\text{SNR}_{\text{train}}$ ) for a particular testing SNR ( $\text{SNR}_{\text{test}}$ ), respectively. Further,  $\bullet$  represents other training SNRs which satisfied the condition given in (8). Interestingly, it reveals significant differences across the different ranges. Particularly, we notice that for most testing SNR values, specially those corresponding to the low SNR regime, the freedom to select the training SNR values that provide close-to-best performance is diminished for higher angle ranges. It can be noticed as well, that positive SNR ranges are in general more favorable. However, when comparing with the results in Fig. 3, we conclude that knowledge of the test SNR favors

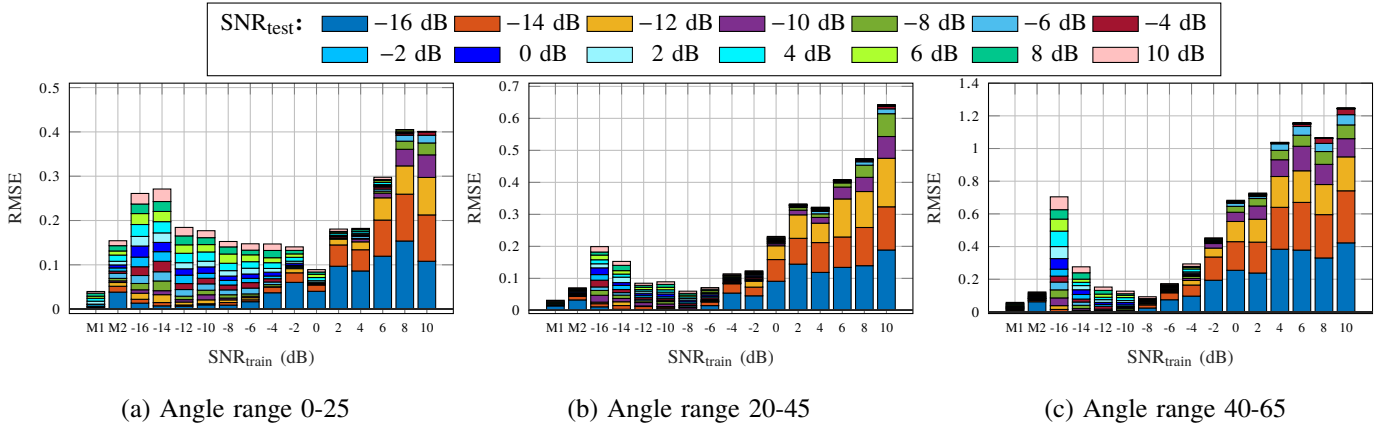


Fig. 5: DOA estimation comparison of the DNN based signal prediction by using all data sets.

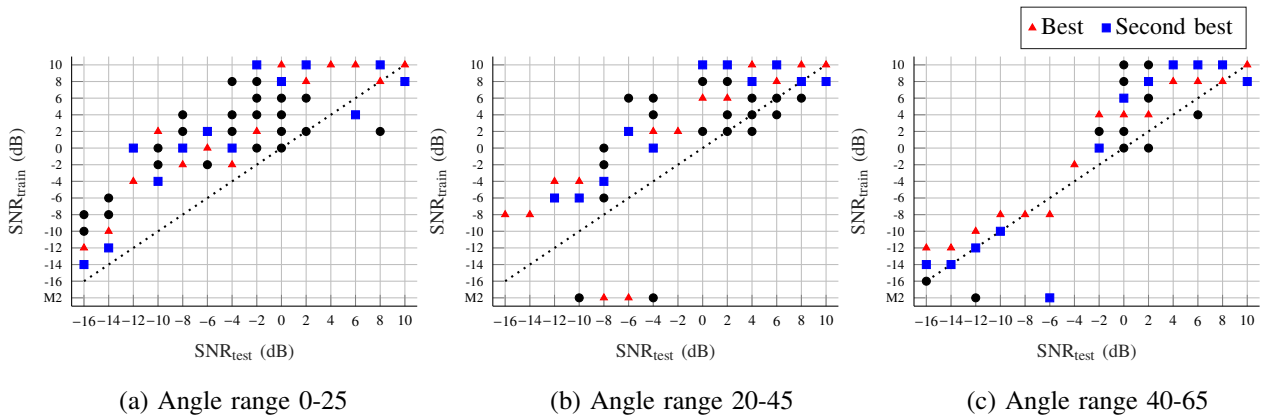


Fig. 6: The best training SNR selection for different test SNRs.

positive training SNR values, while a significant uncertainty about the test SNR favors negative training SNR values.

## V. CONCLUSION

We introduced a novel strategy that employs deep learning for emulating large antenna arrays, and demonstrated how it boosts the accuracy of MUSIC for Direction Of Arrival (DOA) estimation. Multiple observations - of practical significance - were drawn from the obtained results. Most notably, we highlighted how the emulated array leads to superior performance than an actual antenna array with the same number of antennas for large angle ranges and low SNR values, probably due to the denoising abilities of deep neural networks. Further, the effectiveness of training at negative SNR values for large angle ranges in presence of uncertainty about the test SNR was demonstrated. Finally, we investigated the best training SNR range as a function of the test SNR, and particularly noted the sensitivity of performance to the particular choice of the training SNR and with small changes of the test SNR for high angle ranges and low SNR values.

## REFERENCES

- [1] H. L. V. Trees, *Optimum Array Processing: Part IV of Detection, Estimation, and Modulation Theory*. John Wiley & Sons, Ltd, 2002.
- [2] J. Li and P. Stoica, "MIMO radar with colocated antennas," *IEEE Signal Process. Mag.*, vol. 24, no. 5, pp. 106–114, Sep. 2007.
- [3] D. W. Bliss and K. W. Forsythe, "Multiple-input multiple-output (MIMO) radar and imaging: Degrees of freedom and resolution," in *Asilomar Conf. on SSC, 2003*, vol. 1, 2003.
- [4] J. Mietzner, "MIMO arrays versus conventional thin arrays for 2D and 3D radar applications," in *EURAD*, 2017.
- [5] M. Ulrich and B. Yang, "Multi-carrier MIMO radar: A concept of sparse array for improved DOA estimation," in *IEEE Radar Conf.*, 2016.
- [6] A. Moffet, "Minimum-redundancy linear arrays," *IEEE Trans. on Antennas and Propag.*, vol. 16, no. 2, pp. 172–175, 1968.
- [7] P. Pal and P. P. Vaidyanathan, "Nested arrays: A novel approach to array processing with enhanced degrees of freedom," *IEEE Trans. on Signal Process.*, vol. 58, no. 8, pp. 4167–4181, 2010.
- [8] S. Qin, Y. D. Zhang, and M. G. Amin, "Generalized coprime array configurations for direction-of-arrival estimation," *IEEE Trans. on Signal Process.*, vol. 63, no. 6, pp. 1377–1390, 2015.
- [9] D. Khan and K. L. Bell, "Analysis of DOA estimation performance of sparse linear arrays using the Ziv-Zakai bound," in *IEEE Radar Conf.*, 2010.
- [10] P. Pal and P. P. Vaidyanathan, "Coprime sampling and the MUSIC algorithm," in *DSP/SPE*, 2011, pp. 289–294.
- [11] C. Liu and P. P. Vaidyanathan, "Comparison of sparse arrays from viewpoint of coarray stability and robustness," in *IEEE 10th SAM*, 2018, pp. 36–40.
- [12] P. Swerling, "Probability of detection for fluctuating targets," *IRE Trans. on Inf. Theory*, vol. 6, no. 2, pp. 269–308, April 1960.
- [13] D. K. Barton and S. A. Leonov, *Radar technology encyclopedia*. Artech house, 1998.
- [14] P. Ioannides and C. A. Balanis, "Uniform circular arrays for smart antennas," *IEEE Antennas and Propagation Magazine*, vol. 47, no. 4, pp. 192–206, 2005.
- [15] X. Wang, S. Ju, X. Zhang, S. Ramjee, and A. El Gamal, "Efficient training of deep classifiers for wireless source identification using test SNR estimates," *IEEE Wireless Communications Letters*, 2020.